IASS-IACM 2000

Fourth International Colloquium on
Computation of Shell & Spatial Structures

June 4-7, 2000
Chania-Crete, Greece

COMPARATIVE STUDY OF THE GEOMETRIC INCOMPATIBILITIES IN THE DINAMICA OF EXPANDABLE STRUCTURES

Enrique López Hernández, Manuel Muñoz Vidal

Departamento de Tecnoloxía da Construcción, Universidade da Coruña
A Coruña, España
e-mail: lito@udc.es

Key words: expandable, meshes, dynamics, damping, incompatibilities, effort

Abstract. *Expandable meshes are structures built by bars articulated at the extremes and with a passing articulation at the central knot. The calculation of these structures presents numerous difficulties, but furthermore, in many typologies the deployment is influenced by geometric incompatibilities in the intermediate positions that add new and complex factors to their analysis. Although the compatibility limitations have already been studied by several authors for slow-deployable grids by means of a static or quasi-static approach, it is obvious that for temporary structures, speed of erection and dismantling is an important part of the functionality of the product.*

For the study of such phenomena, the authors present a dynamic model of the structural movement, analysing the deployment by means of calculations in the time domain and idealising the actual structure as a model of rigid bars with elastic joints between them. Thus, in our model a bar has 6 co-ordinates corresponding to both end nodes and 5 co-ordinates corresponding to the three displacements and two rotations of the central rod.

One of the first explored possibilities with this method is the study of the phenomena of incompatibility during the process of grid unfolding. To note the importance of this effect we are studying comparatively two similar meshes, but whose geometric incompatibilities are meaningfully distinct. Likewise, we will see the importance that the speed of unfolding has, directly related with the phenomena of damping, in the maximum efforts that support the structure.

1 Introduction

Expandable meshes are adequate for covering surfaces that are flat or that have single curvature. However, when having to cover double curvature surfaces or depending on the shape of the base module of the mesh, there is the problem of the geometry of the unfolding process, in that it is not absolutely guaranteed. This occurs, especially, when using triangle base modules since they add quite a lot of rigidity to the ensemble and they do not possess the flexibility of square base modules in readapting their shape, converting into rhombi, to accommodate to surfaces of double curvature. For this reason, and independently of the incompatibilities of the construction, when covering surfaces of double curvature, as spherical domes [1], with meshes of triangular modules, normally, two stable configurations are possible: the initial and the unfolded. However, the geometry of the intermediate positions is not feasible if taking into account that the bars are straight segments. It must be considered that the bars bend due to flexion. For this same reason, it is not feasible to perform reconstructions of the expandable process from a purely geometric point of view.

2 Definition of the problem

Consider a grid made of bars joined by their ends or by approximately their middle points in an articulated way [2]. If we imagine these joints as elements that form the structure and we suppose that only these elements or nodes are loaded, then their co-ordinates and velocities can describe the movement of the structure. In that case, the equation of movement of the structure can be written as follows [4]:

$$\mathbf{K}.\mathbf{U}+\mathbf{C}+\mathbf{M}.\mathbf{A}=\mathbf{R} \tag{1}$$

where **K** is the stiffness matrix, **U** the nodes co-ordinate matrix, **C** the damping matrix, **M** the nodes mass matrix, **A** the nodes acceleration matrix and **R** the external forces matrix. Continuing with the simplification of the model, we assume the lumped mass model, where the mass matrix has terms corresponding to a specific distribution of the mass of the bar. Within this model, the acceleration depends only on the node co-ordinate and velocity, the external forces and the first neighbours co-ordinates verifying:

$$\mathbf{A}_i = \mathbf{A}_i(\mathbf{U}_i, \mathbf{V}_i, m_i, \mathbf{U}_j, \mathbf{V}_j) \tag{2}$$

being $\mathbf{A_i}$, $\mathbf{U}_i$, $\mathbf{V_i}$ and m_i the acceleration, co-ordinate, velocity and mass of the i-node and $\mathbf{U_j}$ and $\mathbf{V}_j$ the position and velocity of its first neighbours.
The mass distribution is very important in this model and was fitted for adapting it to the grid and for obtaining a compromise between precision and calculation time. Therefore, each bar was divided in three nodes of two different types (Fig.1)
With this kind of modelling we can simulate both the articulated joints of bars at their ends and the typical joint of two bars at an intermediate point. This intermediate point divides, in general, the bar in two different semibars.

An important point to determine is the value of mass point and mass and inertia of the central rod. In our case the mass M and inertia I of the central node was taken as the mass and inertia of a bar of 0.6 times the length of the actual bar. The mass of end nodes was taken proportional to the length associated to each semibar, verifying:

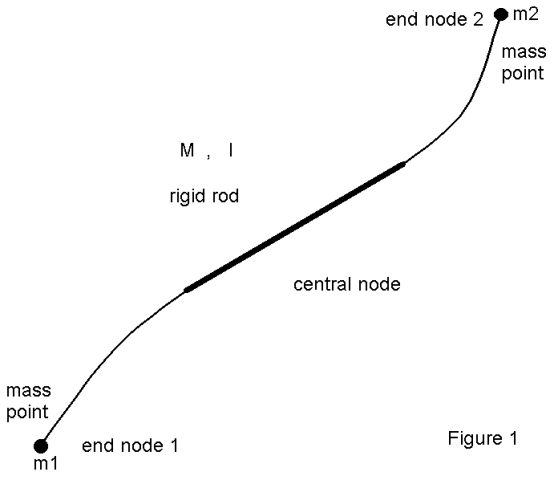

Figure 1

$$M+m1+m2=\text{Mass of the whole bar} \quad (3)$$

Thus, in our model a bar has 6 co-ordinates corresponding to both end nodes and 5 co-ordinates corresponding to the three displacements and two rotations of the central rod.
So, the whole structure will be formed first by point-type nodes with a mass corresponding to the sum of the mass of every semibar that ends in that node and then by rod-type nodes joined by their middle point.
For the modelling of the forces we consider each semibar separately according to Fig.2.
For the values of stresses P, Q and M, the quasi-static approximation is assumed, taking these values from the equilibrium conditions and supposing that they are still valid.

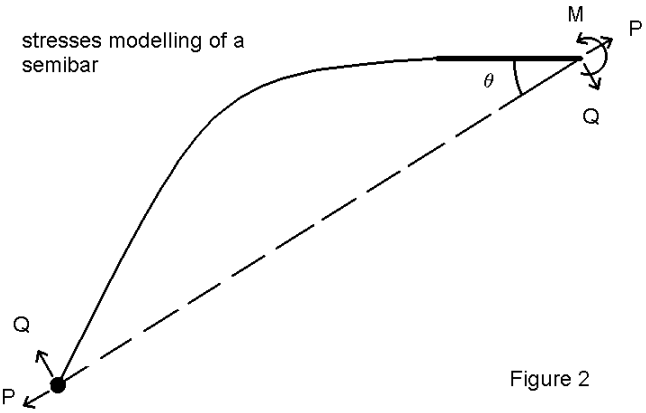

Figure 2

Resulting:

$$P= EA(L-\Delta L)/L \quad (4)$$
$$Q=3EI\theta/L^2 \quad (5)$$
$$M=3EI\theta/L \quad (6)$$

where E is the elasticity module of the material, A the section of the bar, L the length of the semibar, ΔL the variation of the length, I the inertia moment of the section of the bar and θ is the angle in radians. We have neglected torsional effects.
After calculating both semibars, we obtain 6 stresses due to internal forces over the central rod and 2 stresses per end node. Repeating this process for every semibar, and adding the external forces and the stresses coming from their neighbours, we can get both the resultant force that acts over an end node and the force and moment resulting over the central rod.

2.1 Dynamic equations

In the previous section, we explained how the resultant force **R** over an end node and the resultant force **R** and moment **M** over a central node can be calculated. The equation of movement of the i-end node can then be written directly as:

$$\mathbf{A}_i=\mathbf{R}_i/\mathbf{m}_i-\lambda\mathbf{v}_i \quad (7)$$

And, assuming that the central rod can be treated as a one-dimensional rigid body, the five (8, 9, 10) equations of movement of the k-central node become [5] (Fig.3)

$$\mathbf{A_k}=\mathbf{R}_k/\ \mathbf{m}_k\ -\lambda\mathbf{v}_k \tag{8}$$

$$d^2\Theta_k/dt^2=Ma_k/I^*+(d\Phi_k/dt)^2\cos\Theta_k\cos\Theta_k-\lambda d\Theta_k/dt \tag{9}$$

$$d^2\Phi_k/dt^2=(Mc_k/\ I^*-2\ (d\Theta_k/dt)(d\Phi_k/dt)\ \cos\Phi_k)/\sin\Theta-\lambda d\Phi_k/dt \tag{10}$$

where λ is the viscous damping factor, I^* is the inertia of the central rod, m is the mass, Θ and Φ are the Euler co-ordinates of rod k, and Ma and Mc are the projection over the a and c axis of the resultant moment M.
For solving the above mentioned equations, we used the semi-implicit method of Adams-Moulton of fourth order that allows a reasonable balance between precision and calculation time. This method is a two step process, beginning with the prediction step in which the co-ordinates and velocities can be approximated by

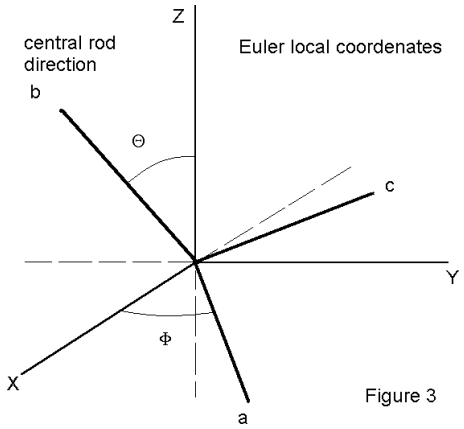

Figure 3

$$u^*(t+dt)=u(t)+dt(55v(t)-59v(t-dt)+37v(t-2dt)-9v(t-3dt))/24 \tag{11}$$

$$v^*(t+dt)=v(t)+dt(55a(t)-59a(t-dt)+37a(t-2dt)-9a(t-3dt))/24 \tag{12}$$

followed by the correction step :

$$v(t+dt)=v(t)+dt(9a^*(t+dt)+19a(t)-5a(t-dt)+a(t-2dt))/24 \tag{13}$$

$$u(t+dt)=u(t)+dt(9v(t+dt)+19v(t)-5v(t-dt)+v(t-2dt))/24 \tag{14}$$

The dt used was of the order of 10^{-5}seg.

3 Meshes studied in this work

In this article, two expandable structures will be analysed. They are relatively similar as far as geometry and general dimensions, characteristics of the bars and load applied, but substantially different in the geometric incompatibilities they undergo during the unfolding process [3]. Possible constructive incompatibilities were not considered.

Common Characteristics: With both, an attempt will be made to cover a 10 m radius spherical dome with an expandable mesh of third order, formed by cross modules having a bar length of approximately 1.80 m. in the folded position. At the beginning of the unfolding process, these modules are not folded in totality, but cover a 10º arch from the pole of the dome. Vertical load

is 10 kg at every node of the upper part, and 30 kg at the lower. To favour unfolding, constant horizontal loads are considered at the upper nodes of the corners, and of 50 kg. that pull in the radial direction. The bars are hollow tubular shapes (4 cm diameter and 2 mm wall thickness) made of steel. During the unfolding process and to facilitate it, the mesh is supported on the lower nodes, adjacent to the central node. In the calculation, the actual weight of the bar is taken into account and correction for axial rigidity as a function of the axial forces applied on the bars is made.

Differences: Because the principal objective of this work is to show the relevance of geometric incompatibilities, a mesh with few or no incompatibilities, as the quadrangular modules type, and another that, a priori, will have significant incompatibilities, as the triangular module, will be chosen.

3.1 Quadrangular module mesh

This mesh was chosen for its few geometric incompatibilities when being unfolded, and a generation process of the mesh that guarantees this.

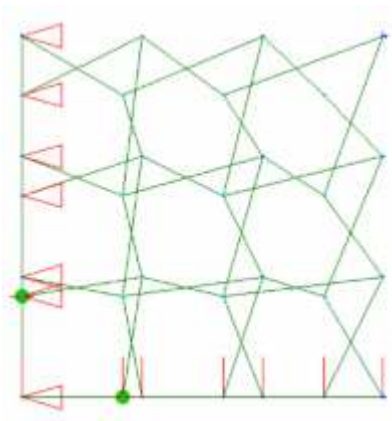

Fig. 4

The generation process consists of starting at a node at the top of the dome. The scheme of the modules is drawn on the surface of the sphere, starting from the two orthogonal meridians that pass through the starting node. The starting length of the module is drawn over these. The next point on the surface of the sphere is located at an equal distance from the two previous points, and so on, such that modules of equal sides are obtained at all times. This form of generation has the advantage that all the bars are of identical length and geometric incompatibility is not present, and the disadvantage that not all modules are similar, being almost square at the top of the dome, and transforming into rhombi at the corners.

The presence of double symmetry has the advantage that only a quarter of the mesh has to be studied. The starting position is nearly the same as in triangular modules, but with the difference that a defined maximum unfolded position is not presented. For this same reason, to maintain it in an unfolded position it will be necessary to fix the edge points, and these will have to guarantee the stability of the unfolded structure.

3.2 Triangular module mesh

This mesh is chosen for its high incompatibility at intermediate positions. The generation process that we have used is based on projecting a flat mesh of equilateral triangles at the equatorial plane, on the spherical surface, using a point proximal to the south pole, located 0.5 m below it, in this case.

To achieve that at the moment of unfolding the angles of all the bars form angles that are similar, the height of the mesh had to be modified progressively. Its maximum is in the area proximal to the upper pole, in this area, the bars having lengths in the order of 2 m, decreasing toward the ends, where the bars have a length of close to 1.60 m.

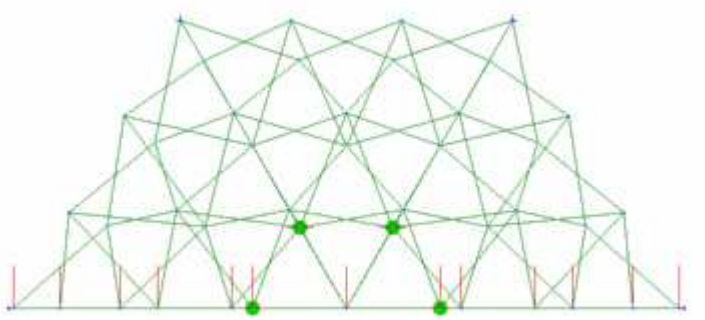

Fig. 5

In the unfolding, the lower points, more proximal to the centre, are used as support, and the symmetry allows having to analyse only half of the mesh. As starting position, a position proximal to total folding is chosen, with a spread of 10º from the pole, as mentioned before, and the unfolded position is set at 80º from pole. In this case, two positions must be defined. The guarantee of geometric compatibility is dependent on these. This is what will help to maintain the unfolded shape, having to fix edge points as in the previous case not being so crucial.

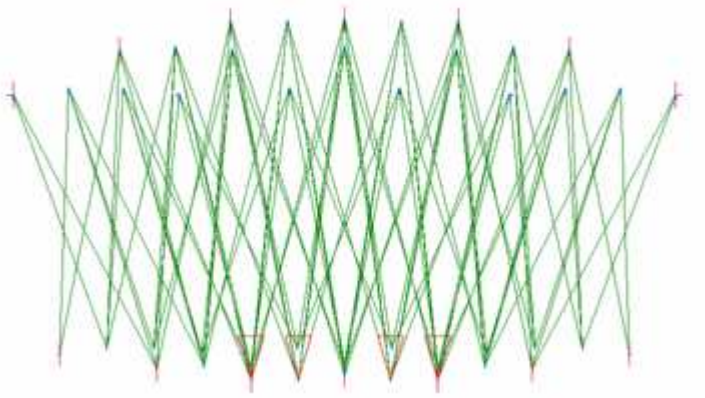

Fig. 6

4 Verification of incompatibilities

Before the calculation process is definite, firstly, we would like to note the different behaviour of both structures during the unfolding process in a trial. For this, we proceed to eliminate vertical loads, except for its own weight (to have precisely the minimum load needed for the unfolding process), and a calculation is carried out assuming damping is null and another with low damping.

The idea of this process is that the loads applied are so low, that when the mesh has a geometric incompatibility, the loads will not be able to overcome it and a “spring back” effect will be produced.

4.1 Quadrangular module mesh

The following graph depicts time in seconds on the x-axis, and the position of a point in metres on the y-axis, and the flexional moment given in the bars. The reference point taken and used for constructing this graph (one of the corners) is continuous, and goes beyond the unfolding point substantially, as the most loaded bars present a flexion of little importance and practically independent of the unfolding process that is becoming more stabilised if we consider a minimum damping of 1 unit (represented on the graph as a01).

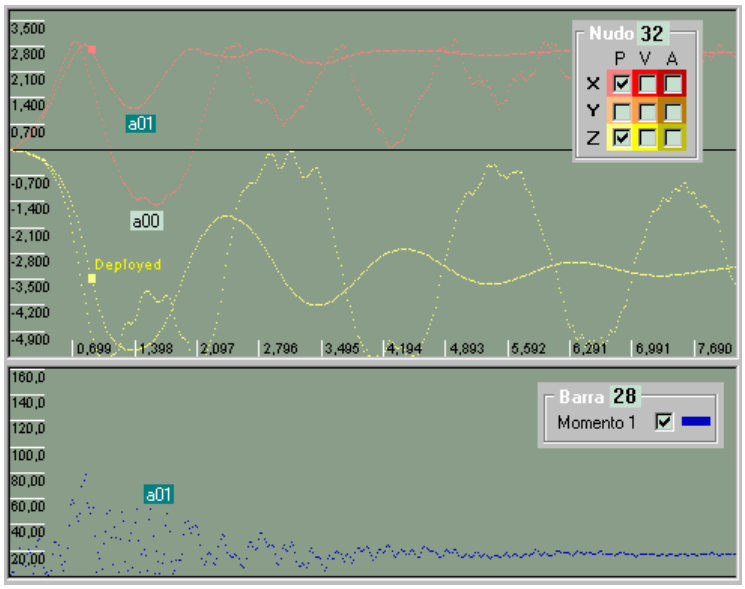

Fig. 7

in the calculation. If damping is null (a00), it enters a repeated cycle, going further beyond the maximum unfolding point and returning, until suddenly reaching the initial point, without flexional forces rising at any particular point.

4.2 Triangular module mesh

In this case, the unfolding process is not completed. In the superior part of the graph, prepared at the same scale as in the previous one, it is observed that the mesh unfolds a bit, but as it continues to unfold incompatibilities are manifested. This creates an increase in the flexional stresses in the bars, and in this case, the external forces cannot overcome the incompatibility zone, producing a "spring back" effect. As observed in the graphs, the differences, in this case as compared with the previous one, are notable: on the one hand, the unfolding process is not achieved and on the other, there is a direct relation of the flexional stresses (to curve the bars in the incompatibility zone, as already mentioned) in the bars with the unfolding position.

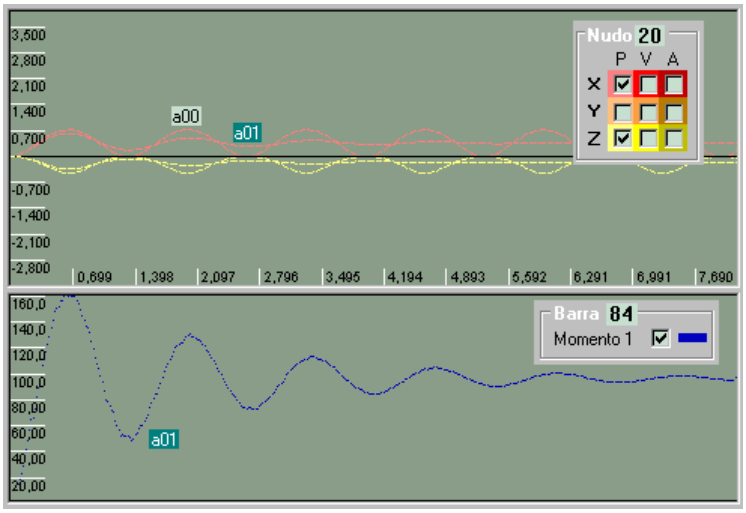

Fig. 8

5 Study of the complete unfolding

This is the principal section of this work, where we will analyse the behaviour of both meshes in a typical unfolding process. We will try to depict, above all, the differences that arise, as far as the forces exerted on the bars and the influence of the degree of damping in this process.

5.1 Quadrangular module mesh

In the study of the unfolding, it is observed that the influence of damping at the time of unfolding the structure is a relation that is quite linear for the damping range studied, although having longer lags as damping is increased.

Axial and flexional stresses as a function of damping (a10... a90) are represented in the following graphs for a bar in the central region (node 28), that is among the most loaded. In both cases, it is observed that the forces vary without excessive abruptness and that the influence that the degree of damping has on the value of maximum forces reached by each of the bars is relatively small.

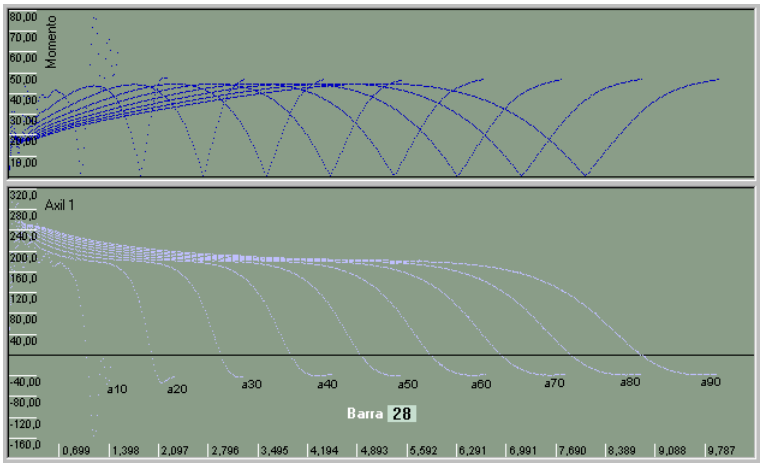

Fig. 9

Precisely, the bars in which the greatest variations appeared are those of the edge, being the ones that present the lowest force values.

Lastly, let us observe the distribution of the axial and flexion forces for an intermediate degree of damping (50) and at a position proximal to total unfolding. It is clearly evident that the bars receiving the most load are those of the central region.

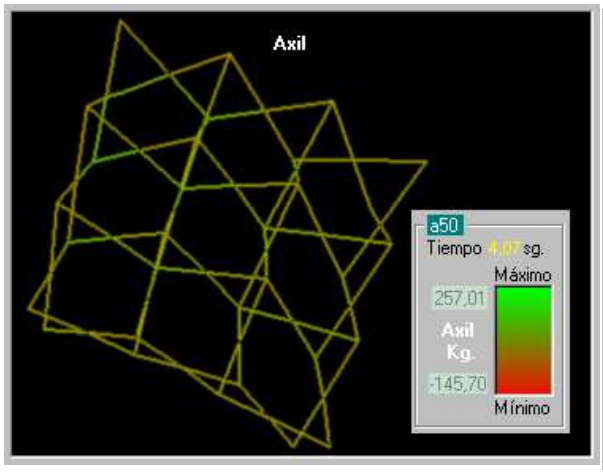

Fig. 10

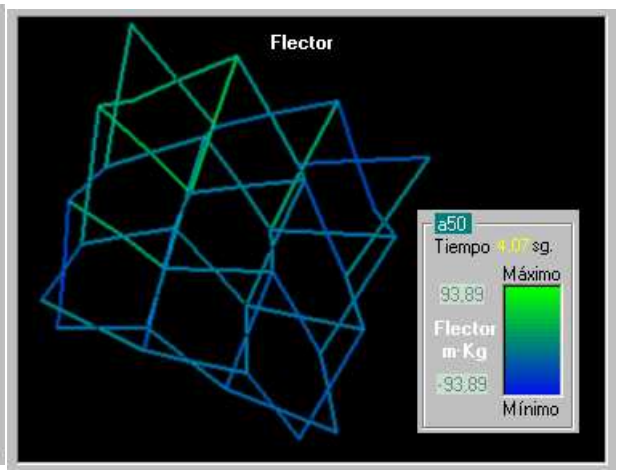

Fig. 11

5.2 Triangular module mesh

As already seen in the study of incompatibilities section, the forces on the bars of this structure are quite related with the geometry of the unfolding. Now, once the unfolding process is completed, this characteristic is observed much better. Additionally, whether the unfolding position is a highly stable position or not is proven since once it is reached, the structure experiences a jolt, as if it stopped suddenly, and remains in this position. This can be perfectly observed in one of the bars near the edge, as no. 84. For simplicity sake, on the graph only damping curves of 10 and 50 have been represented. Here, it is proven that the forces increase notably during the unfolding process until reaching relative maximums or minimums toward the middle of the unfolding, reducing the maximums a bit as damping increases. The "bump" effect is also observed at the end of the unfolding and it remains in this position, that is highly stable. At the moment of the bump, it is also verified that the forces rise less if there is damping that is a bit high.

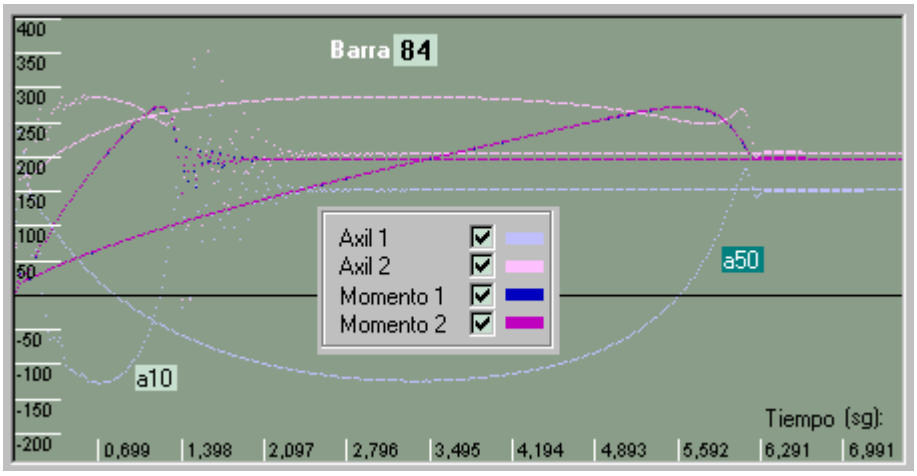

Fig. 12

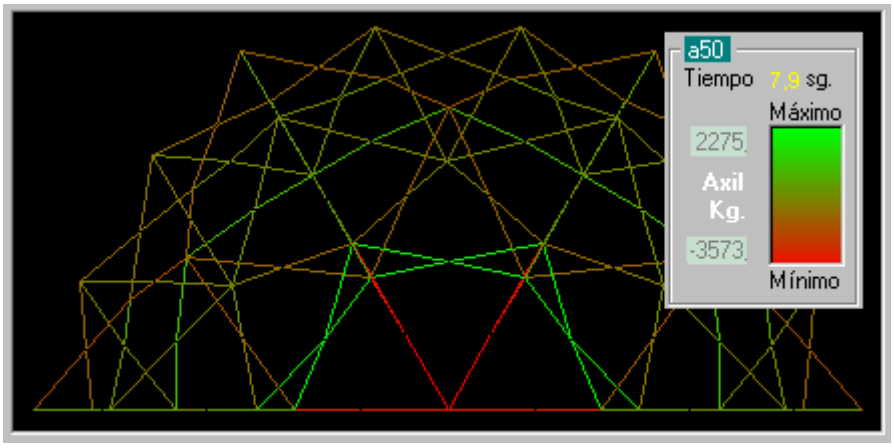

Fig. 13

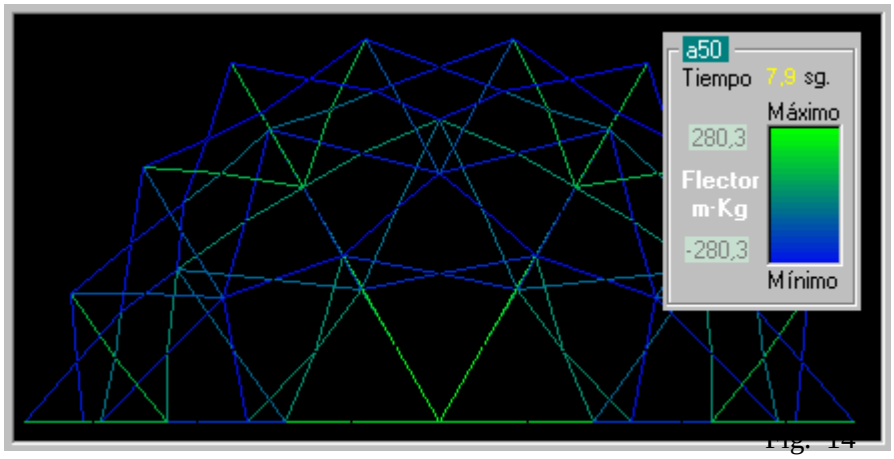

Lastly, we also observe the distribution of axial and flexional stresses for an intermediate degree of damping (50) and at a total unfolding position. As in the

Fig. 14

previous case, it becomes evident that the central bars are the most loaded, although important axial bars are also present at the edge.

5.3 Influence of the geometry on the forces

In the study of the unfolding of this last structure the influence of geometry (incompatibility) is observed in the stresses. Thus, it is interesting to know its relative importance with respect to total forces. For this, we have proceeded with the calculation at the already unfolded position, eliminating all external loads. Because the result of the forces at the final position will depend little on the degree of damping, we have taken an intermediate one, as 30. In the following graphs, this calculation is indicated with **a30** and its continuation with **a31**, where the damping of 30 was maintained.

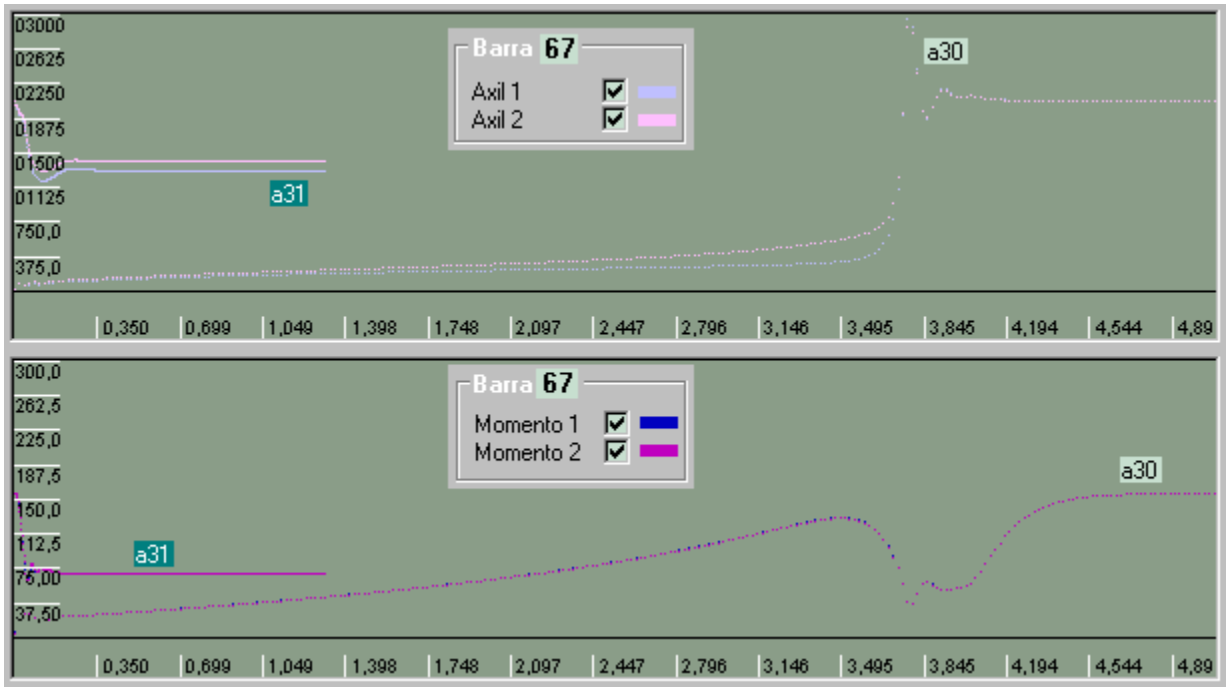

Fig. 15

Los The graphs show axial and flexional stresses of a central bar (bar 67) and one at the edge (bar 84), that correspond with the bars presenting the greatest value during the calculation. The central bar (67) is the one with the greatest axial stresses, that reduce their value by 2/3 (from 2062 to 1400 kg.) once the external loads are eliminated. The moments are reduced to one half, going from 155 to 72 m·kg.

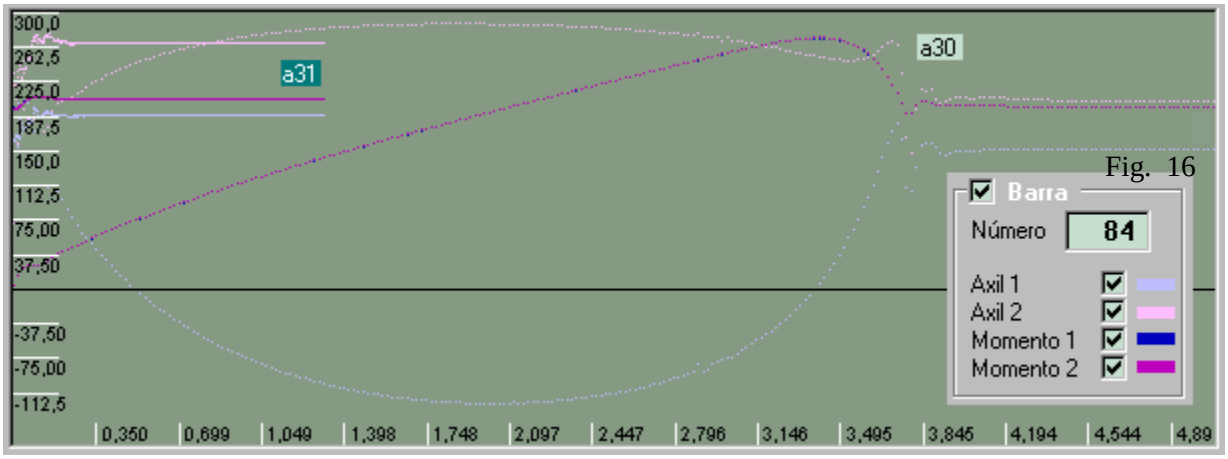

Fig. 16

Fig. 16

At the bar near the edge (bar 84), the axial stresses are much lower, but have greater flexion stresses. Interestingly, the opposite occurs in that when external loads are eliminated the forces of these increase. The axial force goes from 220 to 270, with a 23% increase and the moment increases to a lesser extent, from 190 to 210 (10%).

6 Conclusions

After this analysis, we can conclude that geometric incompatibilities presented by some meshes have a great repercussion on the forces that they will have to support. In some extreme cases, as the one studied, maximum axial forces can be multiplied by 10 and flexional by 3, with the consequent repercussion as far as the greater dimension of the bars and cost, in general. We should note that even when external loads are eliminated, these meshes continue to be loaded, indicating that in many cases it will be the geometry, with its incompatibilities what will generate the greatest part of the forces supported by the bars of this structure.

On the other hand, we should note that structures with strong incompatibilities have advantages as compared to others in that they are highly stable in the unfolded position, in many cases, being able to rely on joining nodes at the edges better than with other meshes.

And lastly, we will note, in meshes with incompatibilities, the importance of damping in maximum forces that it will support, not only during the unfolding, but also at the moment of the "bump" when the final stable position is reached. At this point a low damping factor can produce peaks in the forces that in some cases can duplicate or triplicate those that would be produced with a greater damping.

References

[1] F. Escrig, J. Sánchez and J. Pérez ,"*Two Way Deployable Spherical Grids*". Space Structures, Vol.11, No. 1&2, 1996, pp.257-274
[2] F. Escrig, "*Expandable Space Structures*". Space Structures, Vol.1, No. 2, 1985, pp. 79-91
[3] Y. Rosenfeld and R. Logcher, "*New Concepts for Deployable-Collapsable Stuctures*". Space Structures, Vol. 3, No. 1, 1988, pp. 20-32
[4] A.Ghali and A.Neville, "*Análisis Estructural*". Editorial Diana, Mexico, Chap.15
[5] M. Muñoz and E. López, "*Dynamic behavior of deployable stuctures. Iinfluence of the damping effects in the compatibility limitations of grids*". International Congress ICSS-98. Moscow, RUSSIA.